

# Formal $O(N^3)$ scaling $GW$ calculations by block tensor decomposition for large molecule systems

Yueyang Zhang,<sup>1</sup> Wei Wu,<sup>1</sup> and Peifeng Su\*<sup>1</sup>

The State Key Laboratory of Physical Chemistry of Solid Surfaces, Fujian Provincial Key Laboratory of Theoretical and Computational Chemistry, and College of Chemistry and Chemical Engineering, Xiamen University, Xiamen, Fujian 361005, China

(\*Electronic mail: supi@xmu.edu.cn)

(Dated: 25 December 2025)

Within the framework of many-body perturbation theory based on Green's functions, the  $GW$  approximation has emerged as a pivotal method for computing quasiparticle energies and excitation spectra. However, its high computational cost and steep scaling present significant challenges for applications to large molecular systems. In this work, we extend the block tensor decomposition (BTD) algorithm, recently developed in our previous work [J. Chem. Phys. 163, 174109 (2025)] for low-rank tensor compression, to enable a formally  $O(N^3)$ -scaling  $GW$  algorithm. By integrating BTD with an imaginary-time  $GW$  formalism and introducing a real space screening strategy for the polarizability, we achieve an observed scaling of approximately  $O(N^2)$  in test systems. Key parameters of the algorithm are optimized on the S66 dataset using the JADE algorithm, ensuring a balanced compromise between accuracy and efficiency. Our BTD-based random phase approximation also exhibits  $O(N^2)$  scaling, and eigenvalue-self-consistent  $GW$  calculations become feasible for systems with over 3000 basis functions. This work establishes BTD as an efficient and scalable approach for large-scale  $GW$  calculations in molecular systems.

## I. INTRODUCTION

Many-body perturbation theory (MBPT) based on Green's functions has become a powerful framework for computing ground and excited states in molecule systems.<sup>1,2</sup> In MBPT, the one-body Green's function  $G$  is obtained by solving the Dyson equation, with all correlation effects encapsulated in the self-energy  $\Sigma$ , which plays a role analogous to the exchange-correlation potential in density functional theory (DFT). Hedin's equations provide a systematic and rigorous framework for constructing the self-energy and performing MBPT calculations.<sup>3</sup> The simplest approximation derived from Hedin's equations is  $GW$ ,<sup>4–6</sup> which has been successfully applied in condensed-matter physics for predicting and correcting electronic band structures and is now increasingly applied to molecular systems.

In the  $GW$  approximation, vertex corrections are neglected by setting the vertex functional to unity. For molecular systems,  $GW$  approximation is routinely employed to compute the properties such as HOMO–LUMO gaps and ionization potentials (IPs).<sup>7–12</sup> Rather than performing fully self-consistent  $GW$  (sc $GW$ ) calculations, one often starts with the one-shot  $G_0W_0$  approach. To improve the non-self-consistent  $G_0W_0$  approach, iterative schemes such as eigenvalue self-consistent  $GW$  (ev $GW$ ) and quasiparticle self-consistent  $GW$  (qp $GW$ ) have been proposed.<sup>13–17</sup> Within this hierarchy,  $GW$  becomes an accurate and efficient approach to charged excitation spectra, starting from mean-field reference states to deliver quantitative electronic structure corrections.<sup>18–20</sup> A notable success of the BSE@ $GW$  approach, the combination BSE with  $GW$ , is its ability to accurately describe charge-transfer excitations, which remain challenging for time-dependent DFT (TD-DFT).<sup>21–24</sup>

Although  $GW$ -based methods are computationally more efficient than advanced post-Hartree-Fock methods like coupled

cluster method (CC),<sup>25–29</sup> they are nevertheless more expensive than KS-DFT, hindering their applications to large systems. Without further numerical approximations, the formal scaling of  $GW$  calculations is  $O(N^6)$ . To reduce the cost, many efficient numerical algorithms have been developed to achieve  $O(N^4)$ ,<sup>30,31</sup>  $O(N^3)$ ,<sup>8,32–35</sup> and even linear-scaling by exploring locality or stochastic averaging.<sup>36,37</sup> Among them, low-rank algorithms are particularly effective in reducing computational cost by decomposing electron-electron interactions. Based on the forms of electron-repulsion integral (ERI) factorization, lower-rank algorithms can be divided into three types:

$$\begin{aligned} (\mu\nu|\lambda\sigma) &\approx \sum_M (\mu\nu|\tilde{M})(\tilde{M}|\lambda\sigma) \\ &= \sum_{MN} (\mu\nu|M)(M|N)^{-1}(N|\lambda\sigma) \end{aligned} \quad (1a)$$

$$(\mu\nu|\lambda\sigma) \approx \sum_g X_{\mu g} X_{\nu g} V_{\lambda\sigma}^g \approx \sum_g X_{\lambda g} X_{\sigma g} V_{\mu\nu}^g \quad (1b)$$

$$\begin{aligned} (\mu\nu|\lambda\sigma) &\approx \sum_{KL} X_{\mu K} X_{\nu K} X_{\lambda L} X_{\sigma L} V_{KL} \\ &= \sum_{KL} X_{\mu K} X_{\nu K} X_{\lambda L} X_{\sigma L} \sum_M B_{KMB_{LM}} \end{aligned} \quad (1c)$$

Here eq.(1a) corresponds to the resolution of identity (RI)<sup>38,39</sup> and Cholesky decomposition (CD);<sup>40–43</sup> eq.(1b) represents pseudo-spectral methods<sup>44–51</sup> while eq.(1c) shows the tensor hyper-contraction (THC).<sup>52–58</sup>

These low-rank algorithms have significantly accelerated electronic structure calculations, reducing the computational cost for both DFT and post-Hartree-Fock methods. In MBPT calculations, the use of RI reduces the time scale of  $GW$  from  $O(N^6)$  to  $O(N^4)$  for  $GW$ .<sup>30</sup> THC further reduces the scaling to formal  $O(N^3)$  and has been extended to more advanced MBPT methods beyond  $GW$ .<sup>59,60</sup> Although THC has been successfully applied to periodic  $GW$  calculations,<sup>34,61,62</sup> the applica-

tion in molecular systems is still limited due to the  $O(N^4)$  scaling of the generation for kernel of THC. While cubic scaling has been demonstrated by exploiting locality in basis functions or shell pairs,<sup>33,63–65</sup> the formal scaling with respect to the number of basis functions remains quartic in those implementations.

To overcome the bottleneck of kernel generation, recently, we introduced the block tensor decomposition (BTD) algorithm, a dual-grid THC scheme that achieves formal  $O(N^3)$  scaling in kernel construction.<sup>66</sup> By combining Hilbert space-filling curves with pivoted Cholesky decomposition, BTD generates compact and non-redundant interpolative grids, enabling efficient sparse mapping in real space. This algorithm has been implemented in the calculations of the Hartree-Fock (HF) exchange and the scaled opposite-spin MP2 (SOS-MP2) correlation.<sup>66</sup> In this work, we would like to extend the BTD framework to direct random phase approximation (dRPA) and *GW* for molecule systems.

The motivation of this work is to presents the BTD-*GW* algorithm, which integrates imaginary-time *GW* formalism with BTD low-rank compression and Laplace transformation. This approach achieves formal  $O(N^3)$  scaling, which is further reduced to near-quadratic scaling in practice by leveraging sparsity in the polarizability evaluated on interpolative grids.

The article is organized as follows. In sections II A and II B, we briefly review the imaginary time *GW* with the Laplace transform and the BTD algorithm, respectively. The section II C introduces the algorithm of *GW* based on BTD. In this work, we implement both the one-shot  $G_0W_0$  scheme and the eigenvalue self-consistent ev*GW* scheme<sup>17</sup> within the BTD framework. To assess the precision of the *GW* method, the HOMO energies of the *GW*100 benchmark set are presented in Section III.A. The accuracy of the BTD-based algorithm is examined using the S66×8 test set for non-covalent interactions.<sup>67</sup> Finally, the computational efficiency of BTD-RPA and BTD-*GW* is demonstrated in Section III.B.

## II. METHODOLOGY

The BTD-*GW* algorithm achieves formal  $O(N^3)$  scaling through a systematic strategy: (1) continuous real-space quantities (e.g.,  $G(\mathbf{r}, \mathbf{r}', \tau)$ ) are discretized on a compact set of interpolative grids, (2) these discrete representations are compressed via the block tensor decomposition (BTD), and (3) all subsequent many-body operations (polarization, screening, self-energy) are performed directly on the compressed tensors, avoiding explicit manipulation of high-dimensional intermediates. For clarity, all notations are summarized in Table I.

### A. Imaginary-Time *GW* Formalism with Laplace Transformation

Upon approximating the vertex functional, Hedin's equations simplify to a set of four coupled equations. To avoid divergences along the real-frequency axis, the calculations are

TABLE I: Key notations used in the BTD-*GW* formalism

Notation	Description
$\mu, \nu, \lambda, \sigma$	indices for atomic orbitals (AOs)
$i, j, k, l$	indices of occupied orbitals
$a, b, c, d$	indices of virtual orbitals
$s, t, u, v$	indices of arbitrary orbitals
$g, h$	indices of dense grids
$K, L$	indices of interpolative grids
$M, N$	indices of auxiliary functions for RI
$\tau$	imaginary time
$i\omega$	imaginary frequency
$G$	Green's function
$\Sigma$	self-energy
$\Pi$	polarizability
$W$	dynamical coulomb screening
$\phi_u(\mathbf{r})$	value of orbital on grids
$\chi_M(\mathbf{r})$	value of auxiliary function on grids
$\varepsilon^{QP}$	quasi-particle energy
$D$	density matrix
$C$	coefficient matrix of orbitals

performed on imaginary axis as follows.

$$G(i\omega) = [\mathbf{I} - \mathbf{h}_0 - \Sigma(i\omega)]^{-1} \quad (2a)$$

$$P(\tau) = -G(\tau)G(-\tau) \quad (2b)$$

$$W(i\omega) = \mathbf{v}[\mathbf{I} - \mathbf{v}P(i\omega)]^{-1} \quad (2c)$$

$$\Sigma(\tau) = -G(\tau)W(\tau) \quad (2d)$$

The one-electron Hamiltonian matrix  $\mathbf{h}_0$  in eq. (2a) is the representation of the following operator  $\hat{h}_0$  in the atomic orbital basis shown below:

$$\hat{h}_0 = -\frac{1}{2}\nabla^2 - \sum_a \frac{Z_a}{\mathbf{R}_a} + \int \frac{\rho(\mathbf{r}')}{|\mathbf{r} - \mathbf{r}'|} d\mathbf{r}' \quad (3)$$

The Hedin equations are solved in both the time and frequency domains, with the aim of avoiding complex convolution calculations. The Dyson equations of eq.(2a) and eq.(2c) are solved in the frequency domain. The polarization propagator and self-energy are built in the time domain as eq.(2b) and eq.(2d), respectively.

In the calculations of *GW*, the most time-consuming step is the calculation of dynamical coulomb screening  $W$ . Using RI, polarizability  $\Pi$  and dynamical coulomb screening  $W$  are computed as follows.

$$\Pi_{MN}(i\omega) = \sum_{ia} (M|ia)P_{ia}(i\omega)(ia|N) \quad (4a)$$

$$W_{ia,jb}(i\omega) = \sum_{MN} (ia|M)[\mathbf{I} - \Pi(i\omega)]_{MN}^{-1}(N|jb) \quad (4b)$$

Here  $W_{ia,jb}(i\omega)$  is the dynamically screened Coulomb interaction in the orbital representation; while  $P_{ia}(i\omega)$  is the polarization propagator in the orbital representation, which is defined by eq (5a)

In the zero-temperature limit, the irreducible polarization propagator  $P$  and the Green's functions in orbital representa-

tion are calculated as below:

$$P_{ia}(\tau) = -G_a(\tau)G_i(-\tau) \quad (5a)$$

$$G_a(\tau) = \exp(-\tau\epsilon_a) \quad (\tau > 0 \text{ else } 0) \quad (5b)$$

$$G_i(-\tau) = -\exp(\tau\epsilon_i) \quad (\tau > 0 \text{ else } 0) \quad (5c)$$

The dynamically screened Coulomb interaction  $\mathbf{W}$ , defined in eq. (2c), exhibits different tensor ranks in different representations. In the molecular orbital basis, it is a fourth-order tensor  $W_{ia,jb}(i\omega)$ . In real space representation, however, it reduces to a second-order tensor  $W(\mathbf{r}, \mathbf{r}', i\omega)$ . This is the essential foundation for the subsequent application of low-rank decomposition as THC.

To perform transformations from imaginary time to imaginary frequency and sample points on imaginary axis, many algorithms have been developed for the zero temperature and finite temperature cases.<sup>68–73</sup> In this work, we employ a Laplace-transform based algorithm to connect imaginary-time and imaginary-frequency domains.<sup>70,74,75</sup> Specifically, cosine transforms are applied for the conversions  $\mathbf{P}(\tau) \rightarrow \mathbf{P}(i\omega)$  and  $\mathbf{W}(i\omega) \rightarrow \mathbf{W}(\tau)$ .

$$\mathbf{P}(\omega) = 2 \int_0^\infty \cos(\omega\tau) \mathbf{P}(\tau) d\tau \quad (6a)$$

$$\mathbf{W}(\tau) = \frac{1}{\pi} \int_0^\infty \cos(\omega\tau) \mathbf{W}(i\omega) d\omega \quad (6b)$$

The self-energy is divided into the odd part  $\Sigma^s$  and the even part  $\Sigma^c$ . The sine transformation and cosine transformation are done for odd and even parts, respectively.

$$\begin{aligned} \Sigma(i\omega) = & 2 \int_0^\infty \cos(\omega\tau) \Sigma^c(\tau) d\tau + \\ & 2i \int_0^\infty \sin(\omega\tau) \Sigma^s(\tau) d\tau \end{aligned} \quad (7a)$$

$$\Sigma^c(\tau) = -\frac{1}{2} [\mathbf{G}(\tau) + \mathbf{G}(-\tau)] \mathbf{W}(\tau) \quad (7b)$$

$$\Sigma^s(\tau) = -\frac{1}{2} [\mathbf{G}(\tau) - \mathbf{G}(-\tau)] \mathbf{W}(\tau) \quad (7c)$$

These transformations are efficiently performed by introducing basis functions  $\{\phi_\omega(x)\}$  and  $\{\phi_\tau(x)\}$  to represent functions in the frequency and time domains, respectively:

$$\phi_\omega(x) = \frac{2x}{x^2 + \omega^2} \quad (8a)$$

$$\phi_\tau(x) = \exp(-|\tau|x) \quad (8b)$$

Transformation coefficients are calculated by least-squares minimization.

The calculations of quasiparticle energies require the real-frequency self-energy, which is typically obtained via analytic continuation (AC) or contour deformation.<sup>35,76</sup> In  $G_0W_0$ , the quasi-particle energy of  $u_{\text{th}}$  is calculated with Kohn-Sham orbital  $\phi_u^{KS}$ .

$$\epsilon_u^{OP} = \text{Re} \langle \phi_u^{KS} | \hat{h}_0 + \hat{\Sigma}(\epsilon_u^{OP}) | \phi_u^{KS} \rangle \quad (9)$$

In the eigenvalue self-consistent scheme,  $\{\epsilon_u^{OP}\}$  are used to construct Green's function, and the Hedin's equations are solved iteratively.

The scaling of RI-GW is  $O(N^4)$ . The computational bottleneck is the integral transformation of  $(ia|M)$  and the calculation of  $W_{ia,jb}$ . Explicit construction of the full  $W_{ia,jb}$  matrix would lead to  $O(N^5)$  scaling.

To avoid this quartic and quintic scaling, instead of the orbital representation, the construction of  $W_{ia,jb}$  is reformulated in real space, which provides a more natural framework for exploiting spatial sparsity and enabling low-rank approximations. This strategy avoids the explicit construction of the  $W_{ia,jb}$  matrix and the costly orbital integral transformations. Therefore, the Green's function and the polarization propagator in real space are represented as follows.

$$G(\mathbf{r}, \mathbf{r}', \tau) = \begin{cases} \sum_{i \in \text{occ}} \phi_i(\mathbf{r}) \phi_i^*(\mathbf{r}') \exp(-\tau\epsilon_i); & \tau < 0 \\ -\sum_{a \in \text{vir}} \phi_a(\mathbf{r}) \phi_a(\mathbf{r}') \exp(-\tau\epsilon_a); & \tau > 0 \end{cases} \quad (10a)$$

$$P(\mathbf{r}, \mathbf{r}', \tau) = -G(\mathbf{r}, \mathbf{r}', \tau) G(\mathbf{r}, \mathbf{r}', -\tau) \quad (10b)$$

It is noted that in this work,  $\mathbf{P}$  generically denotes the polarization propagator (density–density response function). In real space representation, we compute  $P(\mathbf{r}, \mathbf{r}', \tau)$  via eq. (10b); after compression onto interpolative grids it becomes  $P_{KL}(\tau)$ . In the molecular orbital representation introduced in eq. (5a), it is denoted as  $P_{ia}$ , and its frequency-domain form  $P_{ia}(i\omega)$  is obtained by Fourier transform of  $P_{ia}(\tau)$ . Projection onto the RI auxiliary basis gives the polarizability matrix  $\Pi_{MN}(i\omega)$ , which appears in both the screened interaction and the RPA correlation energy discussed in the section II C. Thereafter, the BTD algorithm introduced in the section II B is used in the calculations of polarizability.

## B. Block tensor decomposition

In the BTD, electronic integrals are approximated by the interactions of discrete point charges at  $\{\mathbf{r}_g\}$ .<sup>66</sup> These point charges can be contracted to a set of interpolative charges  $\{\mathbf{r}_K\}$  with fewer grids by using overlap fitting.

$$(\mu\nu|\lambda\sigma) = \sum_{KL} X_{\mu K} X_{\nu K} V_{KL} X_{\lambda L} X_{\sigma L} \quad (11a)$$

$$V_{KL} = \sum_{gh} \xi_{Kg} \xi_{Lh} V_{gh} \quad (11b)$$

$$\xi_{Kg} = \sum_L S_{KL}^{-1} \sum_{\mu\nu} Q_g^{\mu\nu} Q_L^{\mu\nu} \quad (11c)$$

$$S_{KL} = \sum_{\mu\nu} Q_K^{\mu\nu} Q_L^{\mu\nu} \quad (11d)$$

$$Q_g^{\mu\nu} = X_{\mu g} X_{\nu g}; Q_K^{\mu\nu} = X_{\mu K} X_{\nu K} \quad (11e)$$

A set of continuous charges is introduced by RI. The point-point interaction  $V_{KL}$  is decomposed into a contraction of two

point-continuum interaction matrices via eq. (12), thereby circumventing the Coulomb cusp  $\lim_{r \rightarrow 0} 1/r$ .

$$V_{KL} = \sum_M B_{KM} B_{LM} \quad (12a)$$

$$B_{KM} = \sum_g \xi_{Kg} B_{gM} \quad (12b)$$

$$B_{gM} = \sum_N (M|N)^{-1/2} \int \frac{\chi_M(\mathbf{r})}{|\mathbf{r} - \mathbf{r}_g|} d\mathbf{r} \quad (12c)$$

BTD employs a dual-grid scheme to replace the computation of 3-center 2-electron (3c2e) integrals with 2-center 1-electron (2c1e) integrals. Compared to other THC schemes for molecular systems, such as least-squares THC (LS-THC),<sup>53</sup> THC-RI,<sup>57</sup> and separable density fitting,<sup>61</sup> BTD exhibits formal cubic scaling with both system size and number of basis functions.

To generate the interpolative points in an efficient and compact way, a scheme based on Hilbert sorting/Octree and pivoted Cholesky decomposition was proposed. This scheme can generate non-redundant grids in a nearly linear-scaling way. The number and distribution of grids are closely related to accuracy and efficiency. To balance efficiency and accuracy, the parameters for dense grids and interpolative grids are optimized by a parameter adaptive differential evolution algorithm named JADE, with details provided in our previous work.<sup>66</sup>

The most time-consuming step of BTD is eq. (12b) with a cost of  $O(N_{\text{aux}} N_K N_g)$ . To reduce time consumption, the sparsity of real space is explored. The sparse map<sup>77–79</sup> between massive grids  $\{\mathbf{r}_g\}$  and interpolative grids  $\{\mathbf{r}_K\}$  is determined by

$$L(\mathbf{r}_g \rightarrow \mathbf{r}_K) = L(\mathbf{r}_g \rightarrow \chi_\mu) \cup L(\chi_\mu \rightarrow \mathbf{r}_K)$$

The cost is reduced to  $O(N_{\text{aux}} N_K)$  as the size of the system grows. The bottleneck is solving the linear equation for overlap fitting with a time scale  $O(N_K^3)$ . In the tests of 1D and 3D systems, BTD shows a scaling between  $O(N^2)$  and  $O(N^3)$ . The implementations of BTD in HF exchange and SOS-MP2 correlation have shown excellent performance.

### C. Formal $O(N^3)$ scaling BTD-GW Algorithm

In this section, by applying BTD, all intermediate quantities are directly computed and compressed on the set of interpolative grids  $\{\mathbf{r}_K\}$ . Specifically, the continuous Green's function  $G(\mathbf{r}, \mathbf{r}', \tau)$  of eq. (10a) is sampled directly on the interpolative grid points to yield the compressed representation  $G_{KL}(\tau)$ . From this, the polarization propagator  $P_{KL}(\tau)$  is constructed via  $P_{KL}(\tau) = G_{KL}(\tau)G_{KL}(-\tau)$ , mirroring the real space relation in eq. (10b). The dynamically screened Coulomb interaction  $W$  is similarly compressed as  $W_{KL}$ . This allows us to efficiently compute the self-energy in the atomic-orbital representation without explicitly constructing the fourth-order tensor  $W_{ia,jb}$ .

In our implementation, the self-energy is divided into the static and dynamic parts, a common practice in GW calculations. The static part,  $\Sigma_x(0)$  is the frequency-independent

Hartree-Fock exchange potential at zero frequency, which can be calculated by chain of spheres for exchange (COSX).<sup>80–84</sup> The dynamic part  $\Sigma_c(i\omega)$ , also known as the correlation self-energy, encapsulates all the frequency-dependent correlation effects arising from the screened interaction  $W$ . To obtain the dynamic correlation self-energy  $\Sigma_c(i\omega)$ , the Green's function is first evaluated on the interpolative grids as  $G_{KL}(\tau)$  by direct sampling of eq. (10). The dynamically screened Coulomb interaction  $W_{KL}(i\omega)$  is then constructed on the same grids as follows:

$$W_{KL}(i\omega) = \sum_{MN} B_{KM} B_{LN} [\mathbf{I} - \Pi(i\omega)]_{MN}^{-1} \quad (13a)$$

$$\Pi_{MN}(i\omega) = \sum_{KL} B_{KM} B_{LN} P_{KL}(i\omega) \quad (13b)$$

The  $\Sigma_c(i\omega)$  can be represented in the orbital representation  $\Sigma_{u,c}(\tau)$  and in the basis representation  $\Sigma_{\mu\nu,c}(\tau)$  via the equations below.

$$\Sigma_{u,c}(\tau) = \sum_{\mu\nu} C_{u\mu} C_{\nu c} \Sigma_{\mu\nu,c}(\tau) \quad (14a)$$

$$\Sigma_{\mu\nu,c}(\tau) = - \sum_{KL} X_{\mu K} X_{\nu L} G_{KL}(\tau) [W_{KL}(\tau) - V_{KL}] \quad (14b)$$

Here, the term  $V_{KL}$  is subtracted to avoid double-counting the static exchange already included in the Hartree-Fock exchange.

In this work, the analytic continuation of  $\Sigma_c(i\omega)$  to the real-frequency axis is performed with the Pade approximation. The Pade coefficients are obtained by fitting  $\Sigma_c(i\omega)$  on the imaginary-frequency grid points, and the resulting rational function is evaluated on the real axis to yield  $\Sigma_c(\omega)$ . The nonlinear equation eq.(9) of quasi-particle energy is solved by linear search. With the dynamically screened Coulomb interaction  $W_{KL}$  available on the interpolative grids, the quasiparticle energies  $\epsilon_a^{\text{QP}}$  are determined, completing one cycle of the GW iteration.

Separately, once the polarizability  $\Pi_{MN}(i\omega)$  is obtained via eq. (13b), the direct random phase approximation (dRPA) correlation energy can be evaluated using the adiabatic-connection fluctuation-dissipation theorem (ACFDT).

$$E^{\text{RPA}} = \frac{1}{2\pi} \int_0^\infty \ln(\det[\mathbf{I} - \Pi(i\omega)]) + \text{Tr}[\Pi(i\omega)] d\omega \quad (15)$$

Our BTD-dRPA implementation captures long-range dispersion interactions with an  $O(N^3)$  scaling, offering computational efficiency superior to many post-SCF methods. We implemented and validated the random phase approximation within the BTD framework (BTD-RPA), which naturally served as a precursor and testing ground for our BTD-GW development. This established the cubic-scaling foundation subsequently extended to the full GW formalism.

The scaling of BTD-RPA is formally cubic and the computational bottleneck is the building of  $\Pi_{MN}(i\omega)$  in eq.(13b). To reduce this cost, a prescreening strategy is introduced that takes advantage of the sparsity of the polarization propagator  $P_{KL}(\tau)$  in the time domain. Only grid pairs  $(K, L)$  with non-negligible  $P_{KL}(\tau)$  values are retained for the correlation

energy calculation, as negligible pairs can be screened out. To enable this screening efficiently, the atomic orbital representation of the Green's functions, as defined in eqs. (16a) and (16b), is employed to naturally exploit their spatial locality.

$$\begin{aligned} G_{KL}^>(\tau) &= - \sum_{\mu\nu} X_{\mu K} X_{\nu L} \left( \sum_{a \in \text{vir}} C_{a\mu} C_{a\nu} \exp(-\tau \epsilon_a) \right) \\ &= \sum_{\mu\nu} X_{\mu K} X_{\nu L} G_{\mu\nu}^>(\tau) \quad (\tau > 0) \end{aligned} \quad (16a)$$

$$\begin{aligned} G_{KL}^<(-\tau) &= \sum_{\mu\nu} X_{\mu K} X_{\nu L} \left( \sum_{i \in \text{occ}} C_{i\mu} C_{i\nu} \exp(\tau \epsilon_i) \right) \\ &= \sum_{\mu\nu} X_{\mu K} X_{\nu L} G_{\mu\nu}^<(-\tau) \quad (\tau > 0) \end{aligned} \quad (16b)$$

Here,  $C_{a\mu}$  is the molecular orbital coefficient. Because of the limitation relationship  $\lim_{\tau \rightarrow 0} G_{\mu\nu}^<(\tau) = D_{\mu\nu}$ ,  $G_{KL}^<(-\tau)$  has a similar local property to the density matrix  $D_{\mu\nu}$ . The prescreening is performed by estimating  $X_{\mu K} X_{\nu L} \max_{KL}(D)$ . To enable efficient prescreening, a representative atomic orbital index  $p_K$  is precomputed for each interpolative grid block  $K$ . This index points to the orbital within the sparse map of block  $K$  that has the largest row norm in the density matrix  $D$ . The maximum possible density matrix element between a pair of blocks  $(K, L)$  can then be efficiently estimated as  $D_{p_K, p_L}$ . This estimation procedure is outlined in the following pseudo-code:

```

REQUIRED:  $L(\mu \rightarrow \mathbf{r}_K)$ ,  $L(\mu \rightarrow \mathbf{r}_L)$ ,  $D$ 
ENSURE:  $\max(D_{\mu\nu})$ 
set  $\text{max\_val} = 0$ ;  $p_K = -1$ 
FOR  $\mu \in L(\mu \rightarrow \mathbf{r}_K)$  :
  IF  $\max(D[\mu, :]) > \text{max\_val}$  : (17)
     $\text{max\_val} = \max(D[\mu, :])$ ;  $p_K = \mu$ 
ENDFOR
determine  $p_L$  for  $\mathbf{r}_L$ 
 $\max_{KL}(D) = D_{p_K, p_L}$ 

```

Here, the index  $p_K$  can be determined before the computation of  $\max_{KL}(D)$ . Using the sparse maps between interpolative grids, the scaling of building  $\Pi_{MN}$  is reduced to  $O(N_{\text{aux}}^2 N_K)$ . A key challenge in the  $GW$  formalism arises from the long-range nature of the screened Coulomb interaction  $\mathbf{W}(\tau)$ , which prevents the direct application of the spatial screening schemes used in DRPA. Consequently, the computation of the self-energy  $\Sigma_u(\tau)$  becomes the dominant cost, scaling as  $O(N_K^2 N_{\text{pas}})$ .

As illustrated in Figure 1, the formal  $O(N^3)$  scaling of the  $evGW$  algorithm arises from the collective scaling behavior of its constituent components. The calculation scheme exhibits an overall  $O(N^3)$  scaling. This formal cubic scaling is a direct result of the BTD compression, which ensures that all other key steps, such as building  $\Pi_{MN}$  and inverting the dielectric matrix, also scale no worse than  $O(N^3)$ .

The calculation procedure of BTD-RPA and BTD- $GW$  is summarized in Figure 2. Starting from a mean-field (HF or DFT) reference, the workflow follows the systematic compression strategy outlined above: molecular orbitals and the

density matrix are projected onto interpolative grids, continuous real space quantities (e.g.,  $G$ ,  $P$ ) are discretized and compressed via BTD, and all subsequent many-body operations are performed directly on the compressed tensors. This integrated pipeline enables the formal  $O(N^3)$  scaling demonstrated in the following section.

**REQUIRED:**  $X_{\mu K}$ ,  $B_{KM}$ ,  $\{\phi_u\}$ ,  $\{\epsilon_u^{KS}\}$

**ENSURE:**  $W_{KL}(0)$ ,  $\{\epsilon_u^{QP}\}$

let  $\epsilon_u^{QP} = \epsilon_u^{KS}$

calculate  $\mathbf{F} = \mathbf{h}_0 + \Sigma_x$  with  $\{\phi_u\}$  using RI-COSX

**DO**

calculate Green's function using eq.(10a)

calculate  $\mathbf{P}(\tau)$  on interpolative grids using eq.(10b)

perform the cosine transform for  $P_{KL}$  using eq.(6a)

**FOR** block pairs with no zero  $P_{KL}$

calculate polarizability  $\Pi_{MN}(i\omega)$  using eq.(13b)

**END FOR**

calculate  $[\mathbf{I} - \mathbf{W}(i\omega)]^{-1}$

perform the cosine transform for  $[\mathbf{I} - \mathbf{W}(i\omega)]^{-1}$  as eq.(6b)

calculate self-energy as  $\Sigma_{\mu\nu}^c(\tau)$  and  $\Sigma_{\mu\nu}^s(\tau)$

perform sine and cosine transforms for  $\Sigma$  using eq.(7)

calculate Pade approximation of  $\Sigma_i(\omega)$

calculate  $\epsilon_u^{QP}$  using eq.(9)

**WHILE** don't converge

calculate dynamical coulomb screening with  $\omega = 0$

FIG. 1: Workflow of the BTD- $evGW$  algorithm

### III. RESULTS AND DISCUSSIONS

#### A. Accuracy Assessment: $GW100$ and $S66$ Benchmarks

The algorithm is implemented in the developing version of XEDA software.<sup>85</sup> The calculations of electron integrals are supported by Libxint which is the electron integral library of XEDA. All calculations were performed on Intel(R) Xeon(R) Gold 6226R CPU @ 2.90GHz. The cc-pVDZ basis set was employed, and DFT calculations were supported by Libxc.<sup>86</sup> The cc-pVDZ-RI basis was used for auxiliary functions.

The accuracy of the BTD-based  $GW$  method is assessed using the  $GW100$  benchmark set,<sup>87-91</sup> which comprises 55 molecules containing the elements C, H, O, N, S, P, F, and Cl. The quasiparticle energies are computed using  $GW$ /cc-pVTZ with six different reference states:  $\omega$ B97X-D, CAM-B3LYP, Hartree-Fock, M06-2X, PBE0, and B3LYP. The calculations of the no-iterative  $G_0 W_0$  and the approximate iterative scheme  $evGW$  are performed.

Figure 3 shows the comparison between the computed quasiparticle HOMO energies from  $GW$  and the experimen-

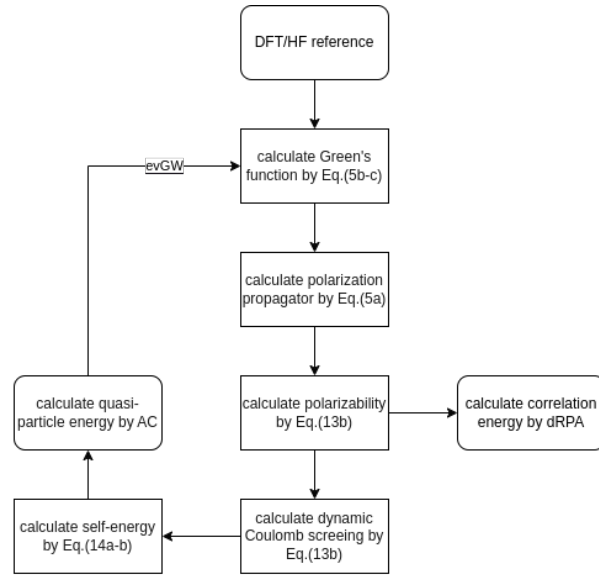


FIG. 2: The procedure of BTD-RPA and BTD-GW

tal vertical ionization potentials (IPs). The original data are shown in Table S1 and Table S2 in the supporting information. The results of  $G_0W_0$  and evGW calculations exhibit a mean absolute error of approximately 1.0 eV. The largest error of about 1.5 eV is observed for tetracarbon ( $C_4$ ). This molecule possesses a significant multi-reference character, with four unpaired electrons coupling to form a singlet ground state. Such a multi-reference character is fundamentally inaccessible to a single-determinant description, whether from restricted HF or KS-DFT. It is important to note that the evGW approach, while self-consistent in the eigenvalues, does not remedy this fundamental issue. As it starts from and iterates upon a single-determinant framework, it primarily captures dynamic correlation and cannot recover the strong static correlation present in  $C_4$ . Consequently, the initial error in the reference state propagates into an inaccurate polarization propagator  $\mathbf{P}$ , leading to the observed deviation.

A detailed analysis of Figure 3 reveals that the effect of the evGW correction varies systematically and significantly with the choice of starting reference. For the hybrid functionals B3LYP and PBE0, the evGW procedure consistently shifts the IPs upward relative to  $G_0W_0$ , leading to a marked improvement. This systematic improvement stems from the fact that the starting Kohn-Sham HOMO-LUMO gap is typically underestimated in these functionals due to their insufficient fraction of exact exchange. The evGW procedure self-consistently updates the quasiparticle energies in the Green's function  $G$ . Through this iteration, the fundamental gap is progressively opened toward the quasi-particle gap, thereby incorporating a more realistic exchange-correlation effect and shifting the IPs upward, which yields better agreement with the experiment data. This mechanism is conceptually analogous to that in the

renormalized single (RS) Green function and the renormalized single-excitation (rSE) in the RPA.<sup>24,92-96</sup>

In contrast, for range-separated functionals  $\omega$ B97X-D and CAM-B3LYP, the  $G_0W_0$  starting point is already accurate, because they approximate the long-range exchange in the  $GW$  self-energy, as shown in Figures 3a and 3b. In such cases, the additional evGW correction can over-adjust the already reasonable gaps, sometimes degrading the performance. The meta-hybrid M06-2X shows the similar behavior, where evGW correction sometimes degrades the result, suggesting a mismatch between its complex functional form and the specific correlation effects addressed by the evGW iteration.

Finally, for HF reference, which lacks dynamic correlation and overestimates the gap, evGW provides the limited improvement because it does not fundamentally rectify the missing correlation in the reference orbitals.

## B. Performance Analysis: Scaling and Efficiency

In order to balance accuracy and efficiency, the parameters of the BTD calculation were optimized on the S66 test set of non-covalent interactions.<sup>97</sup> The reference correlation interaction energies were obtained from RPA@B3LYP/cc-pVQZ calculations. More details of optimization are shown in our previous work.<sup>66</sup> The number of optimization steps is 120 and there are 20 samples in one step. The test data set is chosen as S66 $\times$ 8 and the references are chosen as B3LYP, BLYP and HF.<sup>67</sup> The training process and test results of BLYP reference are shown in Figure 4. The test results of B3LYP and HF are collected in Table S3 and Figure S1 of the supporting information

The mean absolute error (MAE) for the non-covalent interactions in S66 $\times$ 8 is 0.08 kcal/mol, and the maximum error is 0.39 kcal/mol. Benchmark calculations on the S66 $\times$ 8 dataset demonstrate the accuracy of BTD-RPA for non-covalent interactions, with errors sufficiently low for precise relative energy determination. The tests of BTD-RPA at the references of HF and B3LYP, which also show the similar bias.

To assess the computational efficiency of the BTD-based algorithm, BTD-RPA calculations are carried out for glycine chains and water clusters, with timings and energies compared to conventional RI-RPA. The geometries of the Water clusters are taken from our previous work,<sup>66</sup> and those of the glycine chains are taken from literature.<sup>98</sup> The computational consumption of each step and the total times for the BTD-RPA calculations are shown in Figure 5.

For the test systems ranging in size from 300 to 1600 basis functions, the BTD-RPA method exhibits  $O(N^2)$  scaling, which is significantly lower than the  $O(N^4)$  scaling of the RI-RPA approach. The time consumption of BTD-RPA is decomposed into three parts: the generation of the BTD (red), calculation of  $\mathbf{\Pi}(i\omega)$  (green), and computation of correlation energy (blue). The most time-consuming step is to generate the BTD interpolative vector with scaling of  $O(N^{1.5})$ . The calculations of  $\mathbf{\Pi}$  exhibit the cost of  $O(N^{2.0})$  and  $O(N^{2.3})$  for 1D and 3D systems, respectively. The test results show that the BTD-based algorithm is efficient for both 1D and 3D systems.

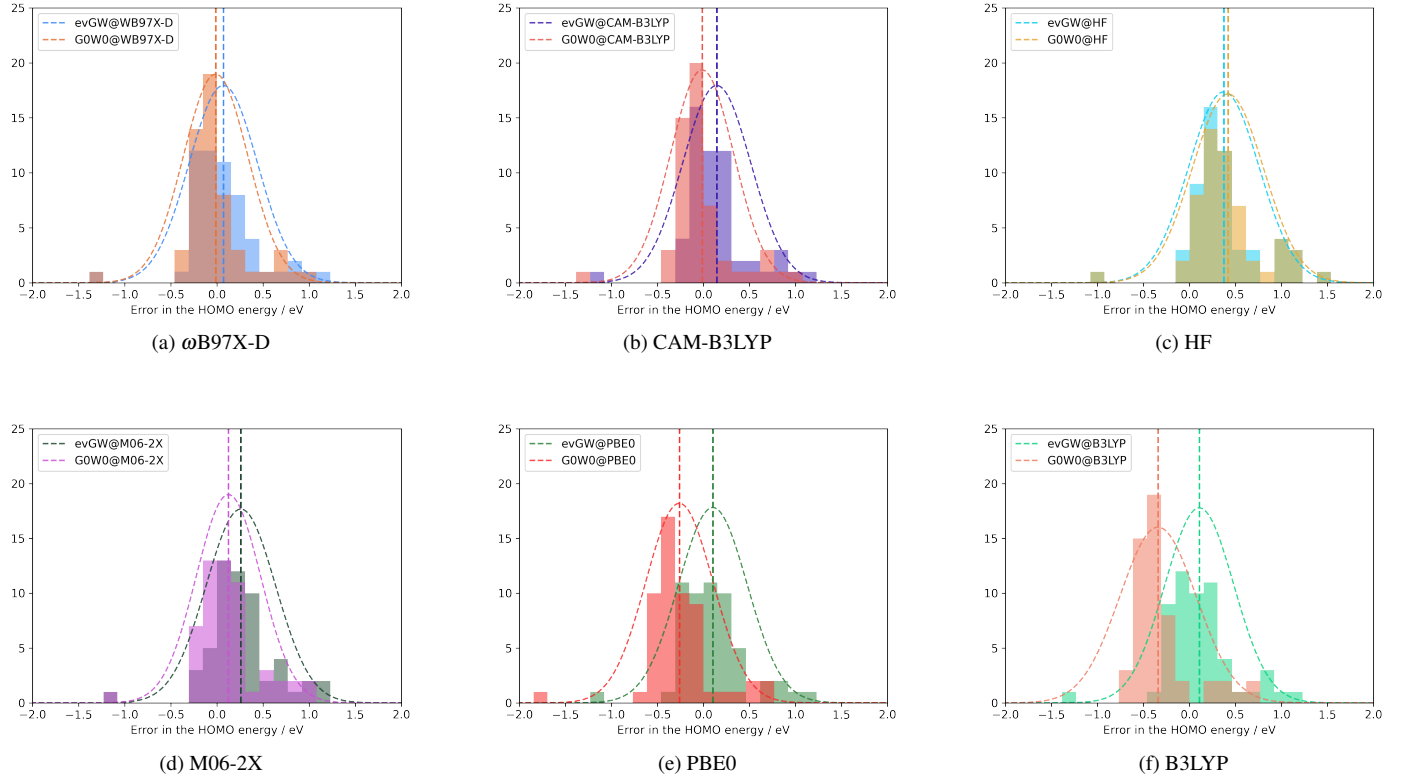


FIG. 3: Deviations of  $G_0W_0$  and evGW HOMO energies from experimental ionization potentials for the GW100 set

The deviations of BTD-RPA from RI-RPA are remarkably small, approximately  $-0.015$  kcal/mol per atom for glycine chains and  $0.05$  kcal/mol per atom for water clusters. This demonstrates that the BTD approximation introduces negligible error in energy evaluations while offering superior computational efficiency.

The scalability of BTD-evGW algorithm is demonstrated by a series of  $\pi$ -conjugated systems in an H-aggregation (face-to-face) stack, as illustrated in Figure 6. The systems range from a single monomer to a heptamer, with the largest system comprising 280 atoms and 3500 basis functions. The values of HOMO and LUMO are shown in Figure S2. The scaling analysis presented in Figure 6 reveals the favorable power-law exponents: approximately  $O(N^{2.5})$  for the BTD kernel generation and  $O(N^{2.8})$  for the self-energy and dynamic screening steps. A BTD-evGW calculation for the largest system (3500 basis functions) converges in five self-consistent cycles and completes in approximately 6000 seconds. This robust performance confirms that our BTD-GW formalism is both efficient and applicable to large-scale molecular systems.

#### IV. CONCLUSION

In summary, we have developed a formally cubic-scaling GW algorithm by integrating the BTD framework with Laplace-transform-based imaginary-time/frequency conver-

sions and analytic continuation. By exploring the sparsity of the density-density response in real space, the time scale can be further reduced to about  $O(N^2)$  for the calculation of  $\Pi$ . The parameters for BTD are optimized on the S66 data set to balance both accuracy and efficiency. The benchmark results confirm that BTD-RPA delivers excellent accuracy for relative energies while achieving sub-quadratic scaling ( $< O(N^2)$ ) for both 1D and 3D systems ranging from 300 to 1600 basis functions. Crucially, our BTD-evGW approximation enables GW calculations for systems with over 3000 basis functions, bringing the practical application of this accurate method to large molecular systems. Future work will also assess the accuracy of BTD-GW for systems containing heavier elements and larger basis sets, further establishing its robustness across various chemical environments.

The BTD-GW quasiparticle energies provide a natural starting point for subsequent Bethe–Salpeter equation (BSE) calculations (BSE@GW), enabling accurate prediction of molecular excitation spectra. When combined with the BTD algorithm for computing the exchange kernel, the BSE@GW approach can also achieve formal  $O(N^3)$  scaling, paving the way for large-scale excited-state calculations. The related work is going on. The calculation of GW still suffers from the long-range performance of the Coulomb interaction. How to screen long-range interaction for self-energy's calculation is still a problem.

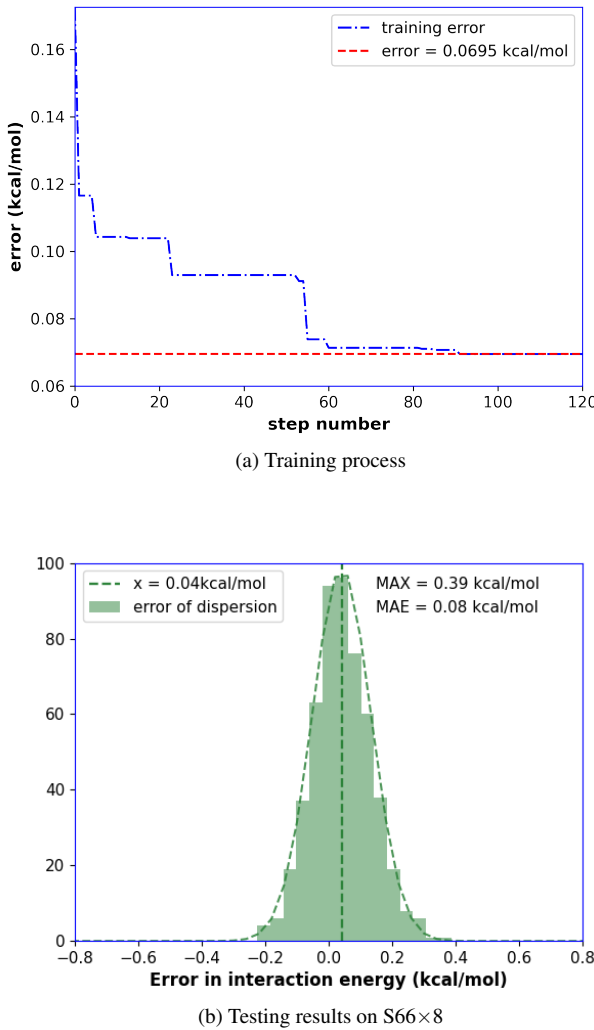


FIG. 4: (a) Training process on S66 test, (b) Error distribution of BTD-RPA compared to RI-RPA on S66×8 with the BLYP reference

## SUPPLEMENTARY MATERIAL

See supplementary material associated with this article, including Tables S1-S3 and Figures S1-S2 and and the zip files of the coordinates for the geometries of aggregations from 1 to 7.

## ACKNOWLEDGMENTS

This project is supported by the National Natural Science Foundation of China (Nos. 22473092, 22173076, 22373077).

## AUTHOR DECLARATIONS

### Conflict of Interest

The authors have no conflict of interest to disclose.

### DATA AVAILABILITY STATEMENT

The data that support the findings of this study are available within the article and its supplementary material.

### REFERENCE

- <sup>1</sup>J. Luttinger and J. Ward, "Ground-state energy of a many-fermion system. ii," *Phys. Rev.* **118**, 1417–1427 (1960).
- <sup>2</sup>G. Baym and L. Kadanoff, "Conservation laws and correlation functions," *Phys. Rev.* **124**, 287–299 (1961).
- <sup>3</sup>L. Hedin, "New method for calculating the one-particle green's function with application to the electron-gas problem," *Phys. Rev.* **139**, A786–A823 (1965).
- <sup>4</sup>D. Golze, M. Dvorak, and P. Rinke, "The gw compendium: A practical guide to theoretical photoemission spectroscopy," *Front. Chem.* **7** (2019), 10.3389/fchem.2019.00377.
- <sup>5</sup>L. Reining, "The gw approximation: content, successes and limitations: The gw approximation," *Wires Comput Mol Sci* **8**, e1344 (2017).
- <sup>6</sup>J. Deslippe, G. Samsonidze, D. Strubbe, M. Jain, M. Cohen, and S. Louie, "Berkeleygw: A massively parallel computer package for the calculation of the quasiparticle and optical properties of materials and nanostructures," *Comput. Phys. Commun.* **183**, 1269 (2012).
- <sup>7</sup>F. Kaplan, M. Harding, C. Seiler, F. Weigend, F. Evers, and M. van Setten, "Quasi-particle self-consistent gw for molecules," *J. Chem. Theory Comput.* **12**, 2528–2541 (2016).
- <sup>8</sup>D. Foerster, P. Koval, and D. Sánchez-Portal, "An o(n3) implementation of hedin's gw approximation for molecules," *J. Chem. Phys.* **135**, 074105 (2011).
- <sup>9</sup>S. Sharifzadeh, I. Tamblyn, P. Doak, P. Darancet, and J. Neaton, "Quantitative molecular orbital energies within a  $g_{w0}$  approximation," *Eur. Phys. J. B* **85** (2012), 10.1140/epjb/e2012-30206-0.
- <sup>10</sup>F. Bruneval and M. Marques, "Benchmarking the starting points of the gw approximation for molecules," *J. Chem. Theory Comput.* **9**, 324–329 (2012).
- <sup>11</sup>M. van Setten, F. Weigend, and F. Evers, "The gw-method for quantum chemistry applications: Theory and implementation," *J. Chem. Theory Comput.* **9**, 232–246 (2013).
- <sup>12</sup>C. Faber, P. Boulanger, C. Attaccalite, I. Duchemin, and X. Blase, "Excited states properties of organic molecules: From density functional theory to the gw and bethe-salpeter green's function formalisms," *Philos. T R Soc. A* **372**, 20130271 (2014).
- <sup>13</sup>M. Shishkin, "Self-consistent gw calculations for semiconductors and insulators," *Phys. Rev. B* **75**, 235102 (2007).
- <sup>14</sup>T. Kotani, M. Schilfgaarde, and S. Faleev, "Quasiparticle self-consistent gw method: A basis for the independent-particle approximation," *Phys. Rev. B* **76**, 165106 (2006).
- <sup>15</sup>O. Backhouse, M. Allen, C. Scott, and G. Booth, "Self-consistent gw via conservation of spectral moments," *J. Chem. Theory Comput.* **21**, 8963–8981 (2025).
- <sup>16</sup>V. Vlček, E. Rabani, and D. Neuhauser, "Simple eigenvalue-self-consistent  $\delta g_{w0}$ ," *J. Chem. Phys.* **149**, 174107 (2018).
- <sup>17</sup>F. Bruneval, N. Vast, and L. Reining, "Effect of self-consistency on quasiparticles in solids," *Phys. Rev. B* **74**, 045102 (2006).
- <sup>18</sup>M. Zhang, Y. Liu, Y.-N. Jiang, and Y. Ma, "Many-body green's function theory for electronic excitations in complex chemical systems," *J. Phys. Chem. Lett.* **14**, 5267–5282 (2023).

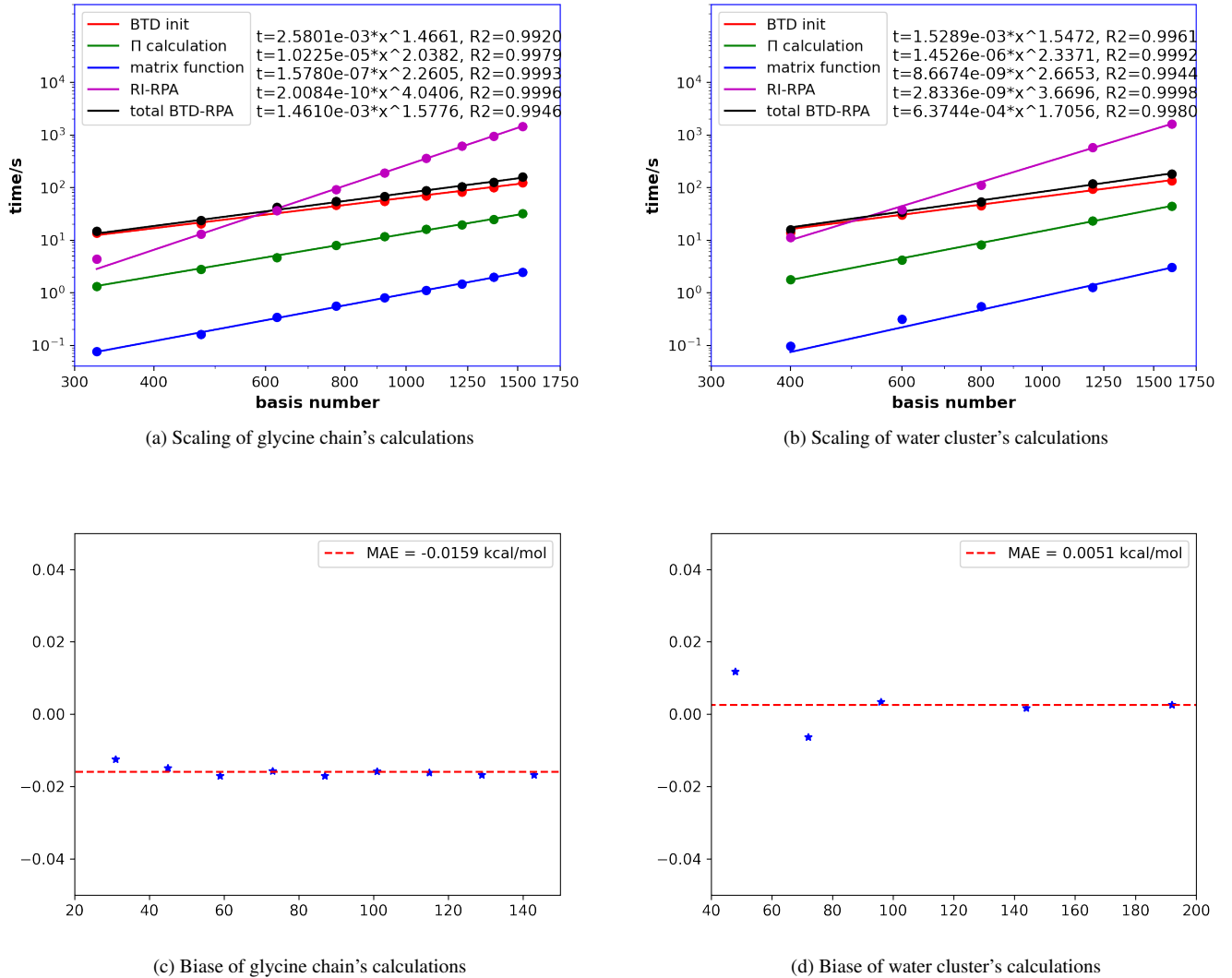


FIG. 5: (a,b) The time costs of glycine chains and water clusters by RI-RPA and BTD-RPA (time of each step is shown); (c,d) the error per atom of BTD compared to RI-RPA.

<sup>19</sup>P.-F. Loos, A. Scemama, and D. Jacquemin, “The quest for highly accurate excitation energies: A computational perspective,” *J. Phys. Chem. Lett.* **11**, 2374–2383 (2020).

<sup>20</sup>G. Onida, L. Reining, and A. Rubio, “Electronic excitations: Density-functional versus many-body green’s-function approaches,” *Rev. Mod. Phys.* **74** (2002), 10.1103/RevModPhys.74.601.

<sup>21</sup>X. Blase, I. Duchemin, D. Jacquemin, and P.-F. Loos, “The bethe-salpeter equation formalism: From physics to chemistry,” *J. Phys. Chem. Lett.* **17**, 7371–7382 (2020).

<sup>22</sup>C. Holzer and Y. Franzke, “A guide to molecular properties from the bethe-salpeter equation,” *J. Phys. Chem. Lett.* **16**, 3980–3990 (2025).

<sup>23</sup>X. Blase, I. Duchemin, and D. Jacquemin, “The bethe-salpeter equation in chemistry: Relations with td-dft, applications and challenges,” *Chem. Soc. Rev.* **47**, 1022–1043 (2018).

<sup>24</sup>J. Li, D. Golze, and W. Yang, “Combining renormalized singles gw methods with the bethe-salpeter equation for accurate neutral excitation energies,” *J. Chem. Theory Comput.* **18**, 6637–6645 (2022).

<sup>25</sup>R. Bartlett and M. Musial, “Coupled-cluster theory in quantum chemistry,” *Rev. Mod. Phys.* **79**, 291–352 (2007).

<sup>26</sup>R. Bartlett, “Perspective on coupled-cluster theory. the evolution toward simplicity in quantum chemistry,” *Phys. Chem. Chem. Phys.* **26**, 8013–8037 (2024).

<sup>27</sup>T. Crawford and H. III, “An introduction to coupled cluster theory for computational chemists,” *Rev Comp Chem* **14**, 33 – 136 (2007).

<sup>28</sup>I. Shavitt and R. Bartlett, *Many-Body Methods in Chemistry and Physics: MBPT and Coupled-Cluster Theory* (Cambridge University Press, 2009).

<sup>29</sup>R. Quintero-Monsobaiz, E. Monino, A. Marie, and P.-F. Loos, “Connections between many-body perturbation and coupled-cluster theories,” *J. Chem. Phys.* **157**, 231102 (2022).

<sup>30</sup>X. Ren, P. Rinke, V. Blum, J. Wieferink, A. Tkatchenko, A. Sanfilippo, K. Reuter, and M. Scheffler, “Resolution-of-identity approach to hartree-fock, hybrid density functionals, rpa, mp2 and gw with numeric atom-centered orbital basis functions,” *New J. Phys* **053020** (2012).

<sup>31</sup>R. Panadés-Barretueta and D. Golze, “Accelerating core-level gw calculations by combining the contour deformation approach with the analytic continuation of w,” *J. Chem. Theory Comput.* **19**, 5450–5464 (2023).

<sup>32</sup>P. Liu, M. Kaltak, J. Klimes, and G. Kresse, “Cubic scaling gw: Towards fast quasiparticle calculations,” *Phys. Rev. B* **94**, 165109 (2016).

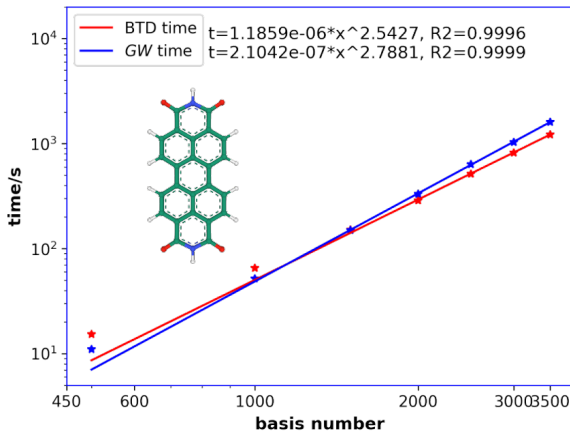


FIG. 6: Scaling of BTD-evGW computational time with system size for  $\pi$ -stacked aggregates (1–7 monomers) with the cc-pVDZ basis set

<sup>33</sup>I. Duchemin and X. Blase, “Cubic-scaling all-electron gw calculations with a separable density-fitting space-time approach,” *J. Chem. Theory Comput.* **17**, 2383–2393 (2021).

<sup>34</sup>C.-N. Yeh and M. Morales, “Low-scaling algorithm for the random phase approximation using tensor hypercontraction with k-point sampling,” *J. Chem. Theory Comput.* **19**, 6197–6207 (2023).

<sup>35</sup>J. Tölle, N. Niemeyer, and J. Neugebauer, “Accelerating analytic-continuation gw calculations with a laplace transform and natural auxiliary functions,” *J. Chem. Theory Comput.* **20**, 2022–2032 (2024).

<sup>36</sup>A. Kutepov, “Self-consistent gw method: O(n) algorithm for polarizability and self energy,” *Comput. Phys. Commun.* **257**, 107502 (2020).

<sup>37</sup>H. Schurkus and C. Ochsenfeld, “Communication: An effective linear-scaling atomic-orbital reformulation of the random-phase approximation using a contracted double-laplace transformation,” *J. Chem. Phys.* **144**, 031101 (2016).

<sup>38</sup>F. Weigendfile;, “A fully direct RI-HF algorithm: Implementation, optimised auxiliary basis sets, demonstration of accuracy and efficiency,” *Phys. Chem. Chem. Phys.* **4**, 4285–4291 (2002).

<sup>39</sup>E. G. Hohenstein and C. D. Sherrill, “Density fitting and cholesky decomposition approximations in symmetry-adapted perturbation theory: Implementation and application to probe the nature of  $\pi$ - $\pi$  interactions in linear acenes,” *J. Chem. Phys.* **132**, 184111 (2010).

<sup>40</sup>N. H. F. Beebe and J. Linderberg, “Simplifications in the generation and transformation of two-electron integrals in molecular calculations,” *Int. J. Quantum Chem.* **12**, 683 – 705 (1977).

<sup>41</sup>I. Røeggen and E. Wistøff-Nilssen, “On the beebe-linderberg two-electron integral approximation,” *Chem. Phys. Lett.* **132**, 154–160 (1986).

<sup>42</sup>I. Røeggen and T. Johansen, “Cholesky decomposition of the two-electron integral matrix in electronic structure calculations,” *J. Comput. Phys.* **128**, 194107 (2008).

<sup>43</sup>T. B. Pedersen, F. Aquilante, and R. Lindh, “Density fitting with auxiliary basis sets from cholesky decompositions,” *Theor Chem Acc* **124**, 1–10 (2009).

<sup>44</sup>R. Friesner, “Solution of self-consistent field electronic structure equations by a pseudospectral method,” *Chem. Phys. Lett.* **116**, 39–43 (1985).

<sup>45</sup>R. Friesner, “Solution of the hartree–fock equations by a pseudospectral method: Application to diatomic molecules,” *J. Chem. Phys.* **85**, 1462–1468 (1986).

<sup>46</sup>R. Friesner, “Solution of the hartree–fock equations for polyatomic molecules by a pseudospectral method,” *J. Chem. Phys.* **86**, 3522–3531 (1987).

<sup>47</sup>M. Ringnalda, M. Belhadj, and R. Friesner, “Pseudospectral hartree–fock theory: Applications and algorithmic improvements,” *J. Chem. Phys.* **93**, 3397–3407 (1990).

<sup>48</sup>T. Martinez, “Pseudospectral multireference single and double excitation configuration interaction,” *J. Chem. Phys.* **102**, 7564–7572 (1995).

<sup>49</sup>J. Langlois, R. Muller, T. Coley, W. Goddard, M. Ringnalda, Y. Won, and R. Friesner, “Pseudospectral generalized valence-bond calculations: Application to methylene, ethylene, and silylene,” *J. Chem. Phys.* **92**, 7488–7497 (1990).

<sup>50</sup>T. Martinez, “Pseudospectral mo/lle–plesset perturbation theory through third order,” *J. Chem. Phys.* **100** (1994), 10.1063/1.466350.

<sup>51</sup>T. Martinez, “Pseudospectral double excitation configuration interaction,” *J. Chem. Phys.* **98**, 7081–7085 (1993).

<sup>52</sup>E. G. Hohenstein, R. M. Parrish, and T. J. Martínez, “Tensor hypercontraction density fitting. i. quartic scaling second- and third-order möller-plesset perturbation theory,” *J. Chem. Phys.* **137**, 044103 (2012).

<sup>53</sup>R. Parrish, E. Hohenstein, T. Martinez, and C. Sherrill, “Tensor hypercontraction. ii. least-squares renormalization,” *J. Chem. Phys.* **137**, 224106 (2012).

<sup>54</sup>E. Hohenstein, R. Parrish, C. Sherrill, and T. Martinez, “Communication: Tensor hypercontraction. iii. least-squares tensor hypercontraction for the determination of correlated wavefunctions,” *J. Chem. Phys.* **137**, 221101 (2012).

<sup>55</sup>X. Qin, W. Hu, and J. Yang, “Interpolative separable density fitting for accelerating two-electron integrals: A theoretical perspective,” *J. Chem. Theory Comput.* **19**, 679–693 (2023).

<sup>56</sup>W. Hu, L. Lin, and C. Yang, “Interpolative separable density fitting decomposition for accelerating hybrid density functional calculations with applications to defects in silicon,” *J. Chem. Theory Comput.* **13**, 5420–5431 (2017).

<sup>57</sup>J. Lee, L. Lin, and M. Head-Gordon, “Systematically improvable tensor hypercontraction: Interpolative separable density-fitting for molecules applied to exact exchange, second- and third-order möller-plesset perturbation theory,” *J. Chem. Theory Comput.* **16**, 243–263 (2019).

<sup>58</sup>K. Dong, W. Hu, and L. Lin, “Interpolative separable density fitting through centroidal voronoi tessellation with applications to hybrid functional electronic structure calculations,” *J. Chem. Theory Comput.* **14**, 1311–1320 (2018).

<sup>59</sup>P. Pokhilko, C.-N. Yeh, M. Morales, and D. Zgid, “Tensor hypercontraction for self-consistent vertex corrected gw with static and dynamic screening; applications to molecules and solids with superexchange,” *J. Chem. Phys.* **162** (2025), 10.1063/5.0269572.

<sup>60</sup>P. Pokhilko, C.-N. Yeh, M. Morales, and D. Zgid, “Tensor hypercontraction for fully self-consistent imaginary-time gf2 and gwsox methods: Theory, implementation, and role of the green’s function second-order exchange for intermolecular interactions,” *J. Chem. Phys.* **161**, 084108 (2024).

<sup>61</sup>J. Lu and K. Thicke, “Cubic scaling algorithms for rpa correlation using interpolative separable density fitting,” *J. Comput. Phys.* **351**, 187–202 (2017).

<sup>62</sup>C.-N. Yeh and M. Morales, “Low-scaling algorithms for gw and constrained random phase approximation using symmetry-adapted interpolative separable density fitting,” *J. Chem. Theory Comput.* **20**, 3184–3198 (2024).

<sup>63</sup>J. Moussa, “Cubic-scaling algorithm and self-consistent field for the random-phase approximation with second-order screened exchange,” *J. Chem. Phys.* **140**, 014107 (2014).

<sup>64</sup>I. Duchemin and X. Blase, “Separable resolution-of-the-identity with all-electron gaussian bases: Application to cubic-scaling rpa,” *J. Chem. Phys.* **150**, 174120 (2019).

<sup>65</sup>E. Spadotto, P. Philipsen, A. Förster, and L. Visscher, “Toward pair atomic density fitting for correlation energies with benchmark accuracy,” *J. Chem. Theory Comput.* **19**, 1499–1516 (2023).

<sup>66</sup>Y. Zhang, X. Xiong, W. Wu, and P. Su, “Block tensor decomposition: A dual-grid scheme with a formal  $O(n^3)$  scale for the decomposition of molecular systems,” *J. Chem. Phys.* **163**, 174109 (2025).

<sup>67</sup>J. Rezac, K. Riley, and P. Hobza, “Extensions of the s66 data set: More accurate interaction energies and angular-displaced nonequilibrium geometries,” *J. Chem. Theory Comput.* **7**, 3466–3470 (2011).

<sup>68</sup>N. Chikano, K. Yoshimi, J. Otsuki, and H. Shinaoka, “irbasis: Open-source database and software for intermediate-representation basis functions of imaginary-time green’s function,” *Comput. Phys. Commun.* **240**, 181–188 (2019).

<sup>69</sup>J. Li, M. Wallerberger, N. Chikano, C.-N. Yeh, E. Gull, and H. Shinaoka, “Sparse sampling approach to efficient ab initio calculations at finite temperature,” *Phys. Rev. B* **101**, 035144 (2020).

<sup>70</sup>M. Kaltak, J. Klimes, and G. Kresse, “Low scaling algorithms for the random phase approximation: Imaginary time and laplace transformations,” *J. Chem. Theory Comput.* **10**, 2498–2507 (2014).

<sup>71</sup>E. Gull, S. Iskakov, I. Krivenko, A. Rusakov, and D. Zgid, “Chebyshev polynomial representation of imaginary-time response functions,” *Phys. Rev. B* **98**, 075127 (2018).

<sup>72</sup>X. Dong, D. Zgid, E. Gull, and H. Strand, “Legendre-spectral dyson equation solver with super-exponential convergence,” *J. Chem. Phys.* **152**, 134107 (2020).

<sup>73</sup>J. Li, M. Wallerberger, N. Chikano, C.-N. Yeh, E. Gull, and H. Shinaoka, “Sparse sampling approach to efficient ab initio calculations at finite temperature,” *Phys. Rev. B* **101**, 035144 (2020).

<sup>74</sup>M. Häser and J. Almlöf, “Laplace transform techniques in molier–plesset perturbation theory,” *J. Chem. Phys.* **96**, 489–494 (1992).

<sup>75</sup>M. Azizi, J. Wilhelm, D. Golze, F. Delesma, R. Panadés-Barrueta, P. Rinke, M. Giantomassi, and X. Gonze, “Validation of the greenx library time-frequency component for efficient gw and rpa calculations,” *Phys. Rev. B* **109**, 245101 (2024).

<sup>76</sup>D. Golze, J. Wilhelm, M. van Setten, and P. Rinke, “Core-level binding energies from gw: An efficient full-frequency approach within a localized basis,” *J. Chem. Theory Comput.* **14**, 4856–4869 (2018).

<sup>77</sup>P. Pinski, C. Riplinger, E. Valeev, and F. Neese, “Sparse maps—a systematic infrastructure for reduced-scaling electronic structure methods. i. an efficient and simple linear scaling local mp2 method that uses an intermediate basis of pair natural orbitals,” *J. Chem. Phys.* **143**, 034108 (2015).

<sup>78</sup>C. Riplinger, P. Pinski, U. Becker, E. Valeev, and F. Neese, “Sparse maps—a systematic infrastructure for reduced-scaling electronic structure methods. ii. linear scaling domain based pair natural orbital coupled cluster theory,” *J. Chem. Phys.* **144**, 024109 (2016).

<sup>79</sup>F. Pavošević, C. Peng, P. Pinski, C. Riplinger, F. Neese, and E. Valeev, “Sparsemaps—a systematic infrastructure for reduced scaling electronic structure methods. v. linear scaling explicitly correlated coupled-cluster method with pair natural orbitals,” *J. Chem. Phys.* **146**, 174108 (2017).

<sup>80</sup>F. Neese, F. Wennmohs, A. Hansen, and U. Becker, “Efficient, approximate and parallel hartree–fock and hybrid DFT calculations. a ‘chain-of-spheres’ algorithm for the hartree–fock exchange,” *Chem. Phys.* **356**, 98–109 (2009).

<sup>81</sup>R. Izsák and F. Neese, “An overlap fitted chain of spheres exchange method,” *J. Chem. Phys.* **135**, 144105 (2011).

<sup>82</sup>R. Izsák, F. Neese, and W. Klopper, “Robust fitting techniques in the chain of spheres approximation to the fock exchange: The role of the complementary space,” *J. Chem. Phys.* **139**, 094111 (2013).

<sup>83</sup>B. Helmich-Paris, B. de Souza, F. Neese, and R. Izsák, “An improved chain of spheres for exchange algorithm,” *J. Chem. Phys.* **155**, 104109 (2021).

<sup>84</sup>Y. Zhang, R. Lei, B. Suo, and W. Liu, “Accelerating fock build via hybrid analytical-numerical integration,” *J. Phys. Chem. A* **129**, 1492–1503 (2025).

<sup>85</sup>Z. Tang, Y. Song, S. Zhang, W. Wang, Y. Xu, D. Wu, W. Wu, and P. Su, “XEDA , a fast and multipurpose energy decomposition analysis program,” *J. Comput. Chem.* **42**, 2341–2351 (2021).

<sup>86</sup>S. Lehtola, C. Steigemann, M. J. Oliveira, and M. A. Marques, “Recent developments in libxc — a comprehensive library of functionals for density functional theory,” *SoftwareX* **7**, 1–5 (2018).

<sup>87</sup>M. van Setten, F. Caruso, S. Sharifzadeh, X. Ren, M. Scheffler, F. Liu, J. Lischner, L. Lin, J. Deslippe, S. Louie, C. Yang, F. Weigend, J. Neaton, F. Evers, and P. Rinke, “Gw100: Benchmarking g0w0 for molecular systems,” *J. Chem. Theory Comput.* **11**, 5665–5687 (2015).

<sup>88</sup>F. Caruso, M. Dauth, M. van Setten, and P. Rinke, “Benchmark of gw approaches for the gw100 test set,” *J. Chem. Theory Comput.* **12**, 5076–5087 (2016).

<sup>89</sup>E. Maggio, P. Liu, M. van Setten, and G. Kresse, “Gw100: A plane wave perspective for small molecules,” *J. Chem. Theory Comput.* **13**, 635–648 (2016).

<sup>90</sup>M. Govoni and G. Galli, “Gw100: Comparison of methods and accuracy of results obtained with the west code,” *J. Chem. Theory Comput.* **14**, 1895–1909 (2018).

<sup>91</sup>A. Förster and L. Visscher, “Gw100: A slater-type orbital perspective,” *J. Chem. Theory Comput.* **17**, 5080–5097 (2021).

<sup>92</sup>Y. Jin, N. Su, and W. Yang, “Renormalized singles green’s function for quasi-particle calculations beyond the g 0 w 0 approximation,” *J. Phys. Chem. Lett.* **10**, 447–452 (2019).

<sup>93</sup>J. Li and W. Yang, “Renormalized singles with correlation in gw green’s function theory for accurate quasiparticle energies,” *J. Phys. Chem. Lett.* **13**, 9372–9380 (2022).

<sup>94</sup>X. Ren, A. Tkatchenko, P. Rinke, and M. Scheffler, “Beyond the random phase approximation for the electron correlation energy: The importance of single excitations,” *Phys. Rev. Lett.* **106**, 153003 (2011).

<sup>95</sup>X. Ren, P. Rinke, G. Scuseria, and M. Scheffler, “Renormalized second-order perturbation theory for the electron correlation energy: Concept, implementation, and benchmarks,” *Phys. Rev. B* **88**, 153003 (2012).

<sup>96</sup>J. Paier, X. Ren, P. Rinke, G. Scuseria, A. Grüneis, G. Kresse, and M. Scheffler, “Assessment of correlation energies based on the random-phase approximation,” *New J. Phys.* **14**, 043002 (2012).

<sup>97</sup>J. Řezáč, K. E. Riley, and P. Hobza, “S66: A well-balanced database of benchmark interaction energies relevant to biomolecular structures,” *J. Chem. Theory Comput.* **7**, 2427–2438 (2011).

<sup>98</sup>Y. Liang, X. Zhang, G. Chan, T. Berkelbach, and H.-Z. Ye, “Efficient implementation of the random phase approximation with domain-based local pair natural orbitals,” *J. Chem. Theory Comput.* **21**, 2918–2927 (2025).